

ULRR

Asymptotic analysis of the dominant mechanisms in the coffee extraction process

Item Type	Article
Authors	Moroney, Kevin M.;Lee, William T.;O'Brien, Stephen;Suijver, Freek;Marra, Johan
Citation	Siam Journal on Applied Mathematics;76 (6), pp. 2196-2217
Publisher	Society for Industrial and Applied Mathematics (SIAM)
Download date	2026-05-15 11:44:54
Item License	https://creativecommons.org/licenses/by-nc-sa/1.0/
Link to Item	https://hdl.handle.net/10344/7239

ASYMPTOTIC ANALYSIS OF THE DOMINANT MECHANISMS IN THE COFFEE EXTRACTION PROCESS*

K. M. MORONEY[†], W. T. LEE[†], S. B. G. O' BRIEN[†], F. SUIJVER[‡], AND J. MARRA[‡]

Abstract. Extraction of coffee solubles from roast and ground coffee is a highly complex process, depending on a large number of brewing parameters. We consider a recent, experimentally validated, model of coffee extraction, describing extraction from a coffee bed using a double porosity model, which includes dissolution and transport of coffee. It was shown that this model can accurately describe coffee extraction in two situations: extraction from a dilute suspension of coffee grains and extraction from a packed coffee bed. Despite being based on some simplifying assumptions, this model can only be solved numerically. In this paper we consider asymptotic solutions of the model describing extraction from a packed coffee bed. Such solutions can explicitly relate coffee concentration to the process parameters. For an individual coffee grain, extraction is controlled by a rapid dissolution of coffee from the surface of the grain, in conjunction with a slower diffusion of coffee through the intragranular pore network to the grain surface. Extraction of coffee from the bed also depends on the speed of advection of coffee from the bed. We utilize the small parameter resulting from the ratio of the advection timescale to the grain diffusion timescale to construct asymptotic solutions using the method of matched asymptotic expansions. The asymptotic solutions are compared to numerical solutions and data from coffee extraction experiments. The asymptotic solutions depend on a small number of dimensionless parameters and so are useful to quickly fit extraction curves and investigate the influence of various process parameters on the extraction.

Key words. double porosity model, coffee brewing process, coffee extraction kinetics, solid-liquid extraction, asymptotic analysis, matched asymptotic expansions

AMS subject classifications. 76S05, 35G20, 41A60

DOI. 10.1137/15M1036658

1. Introduction. Coffee is one of the most widely consumed beverages in the world. This popular drink is made from the roasted seeds (beans) of the coffee plant. Following roasting, the beans are ground, and some of their soluble content is extracted by hot water. This extract is generally filtered to remove undissolved solids, and the resulting solution of hot water and coffee solubles is called coffee. A large number of techniques have been developed for the purposes of brewing coffee for both domestic and catering use. In general, these methods fall into three categories: decoction methods, infusion methods, and pressure methods. Detailed descriptions of many of these brewing procedures are included in [17, 18]. A common feature of all these methods is that they are based on solid-liquid extraction or leaching, which involves the transfer of solutes from a solid (coffee grains) to a fluid (water). Naturally, the target with any of these methods is to consistently produce the best quality coffee possible. First of all, defining what makes a good cup of coffee is a nontrivial matter and to some extent a matter of personal preference. Coffee is composed of over 1800 different chemical components [17]. Such a complex chemistry makes it

*Received by the editors August 24, 2015; accepted for publication (in revised form) September 2, 2016; published electronically November 15, 2016.

<http://www.siam.org/journals/siap/76-6/M103665.html>

Funding: This work was supported by MACSI, the Mathematics Applications Consortium for Science and Industry (www.macsi.ul.ie), funded by the Science Foundation Ireland Investigator Award 12/IA/1683.

[†]MACSI, Department of Mathematics and Statistics, University of Limerick, Limerick, Ireland (kevin.moroney@ul.ie, william.lee@ul.ie, stephen.obrien@ul.ie).

[‡]Philips Research, Eindhoven, 5656 The Netherlands (freek.suijver@philips.com, johan.marra@philips.com).

very challenging to find correlations between the physical parameters of the extracted solubles and the quality of the coffee beverage. In practice coffee quality is usually evaluated by professional coffee tasters. The coffee brewing control chart is often used as a simple alternative measure of coffee quality. This chart gives target ranges for the brew strength and the extraction yield of the coffee based on preferences observed in organized taste tests [19]. Brew strength is the ratio of mass of dissolved coffee in the beverage to volume. Extraction yield is the percentage of dry coffee grind mass that has been extracted as solubles into the water. The second issue is that of the consistency of the brewed coffee. This difficulty arises from the dependency coffee quality has on a large number of process variables. These include the brew ratio (dry coffee mass to water volume used), grind size and distribution, brewing time, water temperature, agitation, water quality, and uniformity of extraction [17, 19]. Clearly a greater understanding of the science of the coffee brewing process and in particular a model of the physics of the extraction process could prove useful in identifying the influence of the various process parameters on the final beverage.

There have been a number of studies into the physics of coffee extraction over the years. Industrial scale coffee extraction processes designed to produce instant coffee have received considerable attention. These systems involve forcing hot water through large packed columns called diffusion batteries, often connected in series, with the aim of extracting a highly concentrated solution. Early work focused on improving the design of these solid-liquid extractors [21, 22]. Much of this work is summarized in [4]. Domestic and catering scale brewing systems have also been the subject of investigation and mathematical modeling. The operation and efficiency of the stovetop or Moka pot have received some experimental investigation [16, 9]. Fasano et al. have developed general multiscale models of coffee extraction, focused primarily on the espresso coffee machine [7, 6, 8, 5]. This multiscale approach is reflective of the presence of multiple length scales in the coffee bed due to its double porosity nature. Large pores exist between the grains, while smaller pores exist within the grains. The porous nature of coffee grains can be seen in scanning electron microscope (SEM) images of coffee grains such as those in [13, 19]. A schematic of the espresso system is shown in Figure 1a. Voilley and Simatos [24] performed a number of different extraction experiments on a well-mixed system of coffee grounds and water. The influence of process parameters such as brewing time, granule size, brew ratio, and water temperature on brew strength was investigated. A simple model was used to describe the variations of brew strength during the extraction experiments. The coffee grains were assumed to be spherical and suspended in a homogeneous system. The extraction was modeled as diffusion of a single component from a sphere, with a diameter equal to the mean grain diameter. Using the diffusion coefficient as a fitting parameter, the model was found to provide reasonable agreement with the data.

The physics of the brewing process in the drip filter brewing system has received very little attention. This is surprising as drip filter machines account for approximately 10 million out of a total of over 18 million coffee machines sold in Europe each year [3]. In the drip filter brewing system, hot water is poured over a bed of coffee grounds contained in a filter. The water flows through the bed under the influence of gravity and extracts coffee solubles from the grains. A schematic of the process is shown in Figure 1b. There are many interesting questions regarding the brewing process in a drip filter system. Some of these questions were investigated by a group of applied mathematicians at the ESGI 87 study group with industry at the University of Limerick [2]. Issues considered included the evolution of the shape of the coffee bed during brewing, correlations between the final shape of the bed and coffee quality, and

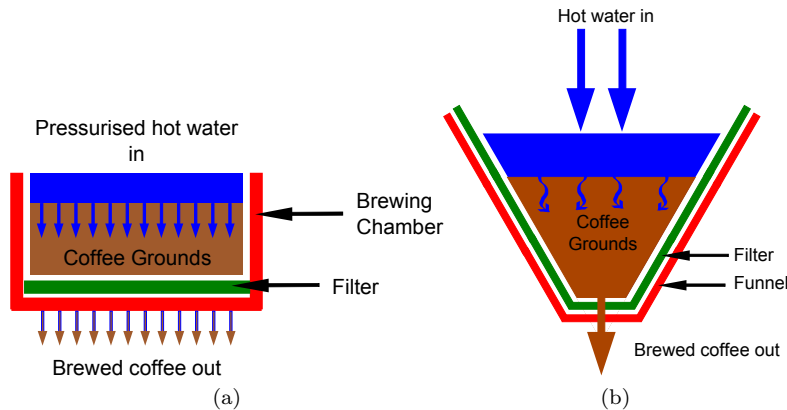


FIG. 1. (a) Espresso coffee is made by forcing hot water under high pressure through a compacted bed of finely ground coffee. (b) Drip filter brewing involves pouring hot water over a loose bed of coarser coffee in a filter. In either method water flows through the bed, leaching soluble coffee components from the grains. Any undissolved solids in the fluid are filtered from the extract as the liquid leaves the filter.

the use of a single jet or multiple jets (shower head) to add water to the coffee bed. In a recent paper, Moroney et al. [14] outlined a new multiscale model of coffee extraction from a coffee bed. This model was motivated by observations in coffee extraction experiments. It was noted that extraction seemed to proceed in two stages: an initial rapid extraction over a short period followed by a much slower extraction during the rest of the brewing time. These observations were explained by assuming that the rapid extraction was occurring due to reduced mass transfer resistances from fine particles and broken coffee cells (due to the grinding process) on the surface of larger grains. The slower extraction was explained by an increased mass transfer resistance from the intact coffee cells in the kernels of larger coffee grains. Numerical solutions of the model equations showed that the model could quantitatively reproduce the extraction profiles from experiment.

In this paper the coffee extraction model introduced in [14] is analyzed. The model is nondimensionalized to identify the dominant mechanisms during coffee extraction. Approximate solutions can be found based on the dominant mechanism of extraction during different stages of the brewing process. Solutions can be found for both fine and coarse grinds in the two experimental situations outlined in [14]. This paper focuses on developing approximate solutions for coffee extraction from a flow-through cylinder similar to that found in an espresso machine, except the water is at a much lower pressure. In this case, solutions for extraction of fine and coarse grinds differ due to a difference in the assumed initial coffee concentration in the coffee bed. Solutions presented are for fine grind parameters. Such solutions can be used to predict the coffee quality (coffee concentration and extraction yield) for a particular brewing configuration with a given set of process parameters. Approximate solutions can also be found for extraction of coffee in a French press-type cylinder. The solution in this case is the subject of a separate paper.

2. Coffee extraction from a fixed cylindrical bed.

2.1. Coffee extraction experiments. The second coffee experiment outlined in [14] involves the extraction of coffee in a cylindrical brewing chamber of a flow-

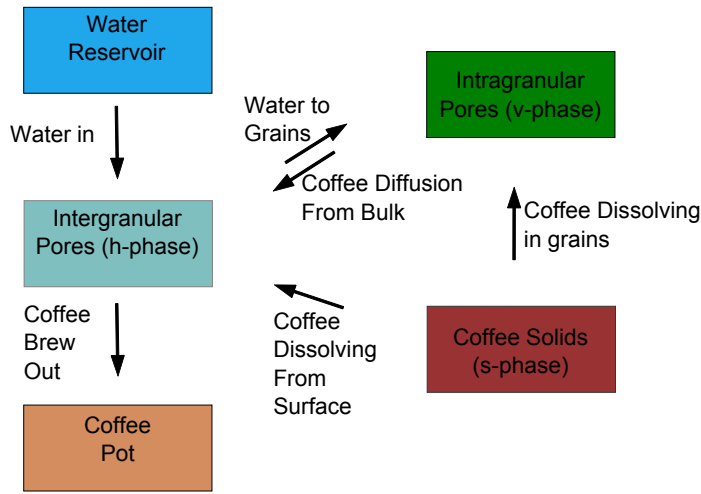


FIG. 2. Transfers included in the coffee extraction model (reproduced from [14]): The diagram shows the transfers of water and coffee which are described by the coffee extraction model presented in [14].

through cell. In this experiment, coffee is placed in a cylindrical flow cell, and 1 L of water at 90 °C is forced through the coffee bed by a rotary vane pump. The set-up closely resembles that in Figure 1a. The coffee beverage exiting from the chamber is collected in a coffee pot. The solubles' concentration of the exiting coffee and the coffee in the pot is measured throughout extraction. This experiment was conducted for a number of different coffees. The focus here will be on the results for one fine and one coarse grind presented in [14]. The coffee bed is static, and the grind size distribution, bed dimensions, flow rates, and pressure drop across the bed are all measured. Full experimental details are included in [14].

2.2. Mathematical modeling of coffee extraction experiment. A general model for extraction of coffee from a static bed of porous grains is derived and described in detail in [14]. This model is specialized to describe extraction from a cylindrical brewing chamber, and some initial numerical results are presented. In this section, the one-dimensional form of the general equations will be presented for a coffee bed of height L . The model equations will be described. The key assumptions made in [14] will be expanded upon and discussed.

A key feature of the model in [14] is that the coffee bed is represented by a porous medium domain using a double porosity model. This means the coffee bed consists of grains which are themselves porous. Isothermal conditions are assumed during brewing as the temperature variations considered are small, and so the variation in any temperature dependent parameters is considered negligible. Although the extraction rate and the percentage of extractable mass increase with temperature [11], optimal brewing conditions require a narrow temperature range in the bed (91 °C to 94 °C [19]). Thus the assumption of isothermal conditions seems reasonable. It should be noted, however, that large temperature variations within the bed may lead to a nonuniform extraction. The infiltration of water into the grains during initial wetting stages is possible due to roasting, which increases the grain permeability due to formation of new pores through cracking [20], and grinding, which decreases the average grain size. The model assumes that all pores in the coffee bed are saturated with fluid and so

does not model unsaturated flow during the initial water infiltration or final draining stages of the brewing process.

Due to the cylindrical geometry of the coffee bed and nature of the flow, we assume that the coffee bed properties are homogeneous in any cross section, so the equations can be reduced to one spatial dimension. This is the coffee bed depth, which we label with the z -coordinate. The height of the coffee bed is L , with the bottom (filter exit) at $z = 0$ and the top (filter entrance) at $z = L$. The transport of coffee and liquid in the coffee bed is modeled by a set of conservation equations on the bed scale. The macroscopic model consists of conservation equations for coffee and liquid in three phases. The phase consisting of the pores between the coffee grains (intergranular pores) is called the h -phase. The coffee grains are also porous. The pores within the grains (intragranular pores) make up the v -phase. Finally the solid coffee matrix in the grains is called the s -phase. The mechanisms in the model through which the transport of fluid and coffee solubles, within and between these phases, occurs are represented in Figure 2.

The coffee concentrations (mass per unit volume) in each of the phases are c_h^* , c_v^* , and c_s . The concentration (density) of the solid coffee matrix c_s is assumed constant. As coffee dissolves it is assumed that the grain porosity changes rather than the solid concentration. Note that dimensional variables are indicated by an asterisk. The porosity (volume fraction) of the intergranular pores is denoted by ϕ_h and is also assumed constant. The volume fraction of the grains ($1 - \phi_h$) is split into two domains. The intragranular pores have a volume fraction (of the total grain volume) of ϕ_v^* , while the solid coffee matrix has a grain volume fraction of $\phi_s^* = 1 - \phi_v^*$. The coffee volume fraction is further divided into three parts, as illustrated in Figure 3. First there is a volume fraction of coffee which is insoluble under the conditions in the coffee bed $\phi_{s,i}^*$, which can depend on water temperature, coffee grind distribution, and other variables. For example, for water at 90 °C the extractable mass in coffee grains can vary from 28% for coarse grinds to 32% for fine grinds of the same coffee [14]. The extractable coffee grain volume fraction is divided into two parts according to its location in the coffee grains. The coffee grind distribution can contain a significant volume of fine grains, which are broken cell fragments produced during grinding of the coffee beans. After the grinding process, the surfaces of the coffee grains consist mostly of broken coffee cells. Coffee in each of these locations is expected to have a significantly lower mass transfer resistance than that in intact cells in the kernels of larger grains. The volume fraction of this coffee is denoted $\phi_{s,s}^*$. The kernels of larger grains consist of intact cells with a much higher mass transfer resistance. The volume fraction of this coffee is denoted $\phi_{s,b}^*$. The volume fraction of soluble coffee in the coffee grains is $\phi_c^* = \phi_{s,s}^* + \phi_{s,b}^*$. It is useful to define the fraction of the original amount of coffee (in the dry coffee grains) remaining in the grain surfaces and in the grain kernels at a given time. The volume fractions of coffee in the dry coffee grains, grain surfaces, and grain kernels are denoted by ϕ_{cd} , $\phi_{s,sd}$, and $\phi_{s,bd}$, respectively. The fractions of the original amount of coffee left on the grain surfaces and in the grain kernels are denoted by ψ_s^* and ψ_v^* .

The surface area of the coffee grain distribution is a key parameter influencing both liquid flow and extraction of coffee during the brewing process. The surface area per unit volume of the entire grain distribution, which influences flow and extraction of coffee from grain surfaces, is described using the Sauter mean diameter k_{sv1} . The Sauter mean diameter is defined as the diameter of a spherical particle which has the same surface area to volume ratio as the grind size distribution under consideration [10]. The surface area per unit volume of larger grains (diameter larger than 50 μm),

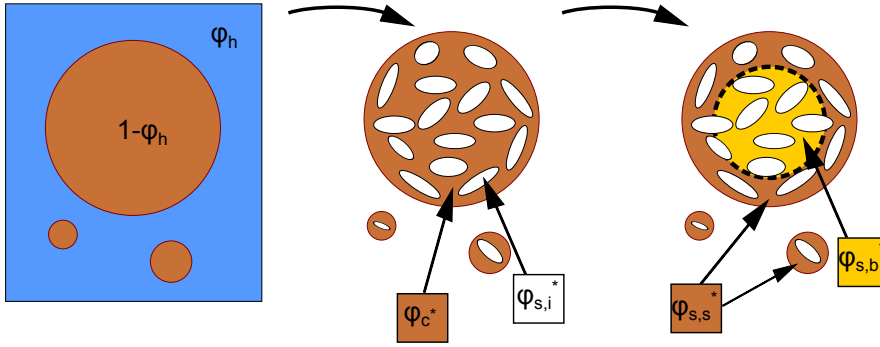


FIG. 3. Location of coffee in the bed: The coffee bed consists of (intergranular) pores of volume fraction ϕ_h and grains of volume fraction $1 - \phi_h$. The grains consist of (intragranular) pores of volume fraction ϕ_s^* and solids of volume fraction $1 - \phi_s^*$. The schematic shows the breakdown of this coffee in the grains (intragranular pores are not represented for clarity). The solid consists of a soluble volume fraction ϕ_c^* and an insoluble volume fraction $\phi_{s,i}^*$. The soluble volume fraction is broken into a volume fraction near the surface of grains $\phi_{s,s}^*$ and a volume fraction in the kernels (bulk) of grains $\phi_{s,b}^*$.

which influences extraction from the kernels of these larger grains, is described using the Sauter mean diameter k_{sv2} . The average coffee cell radius is given by m . The effective diffusion coefficient of coffee in water is given by D_h in the h-phase and D_v in the v-phase. The effective diffusion distance between the v-phase and the h-phase is given by l_l . It is assumed that there is a coffee concentration c_{sat} which is the concentration in the liquid phase that would be in equilibrium with the concentration in the solid phase. This is taken here to be the maximum solubility of coffee in the liquid. Mechanical dispersion can be an important factor in flows in porous media [1]. The dispersion coefficient is denoted by D^b . Other important parameters include the fluid density ρ , the dynamic viscosity of the fluid μ , and the shape factor κ from the Kozeny–Carman equations [10]. The Kozeny–Carman equations are used to relate the bed permeability to its porosity. The fluid pressures in the h-phase and v-phase are p_h^* and p_v^* , respectively. The system of equations in [14] includes a term for transfer of fluid between the h-phase and the v-phase due to differences in pressures. This correction is thought to occur much faster than other processes in the coffee bed and is difficult to model accurately without further experimental insight. For this reason these terms are neglected in the analysis here, which corresponds to the assumption $p_h^* = p_v^*$ at every point in the bed. Thus, neglecting these terms, the general one-dimensional model becomes

$$(2.1) \quad \frac{\partial c_h^*}{\partial t^*} = \frac{k_{sv1}^2 \phi_h^2}{36\kappa\mu(1 - \phi_h)^2} \frac{\partial}{\partial z^*} \left(c_h^* \left(\frac{\partial p_h^*}{\partial z^*} + \rho g \right) \right) + \phi_h^{\frac{1}{3}} D_h \frac{\partial^2 c_h^*}{\partial z^{*2}} \\ + D^b \frac{\partial^2 c_h^*}{\partial z^{*2}} - \alpha^* \frac{(1 - \phi_h)}{\phi_h} \phi_v^{*\frac{4}{3}} D_v \frac{6}{k_{sv2} l_l} (c_h^* - c_v^*) \\ + \beta^* \frac{(1 - \phi_h)}{\phi_h} \frac{12 D_h \phi_{cd}}{k_{sv1} m} (c_{\text{sat}} - c_h^*) \psi_s^*,$$

$$(2.2) \quad \frac{\partial^2 p_h^*}{\partial z^{*2}} = 0,$$

$$(2.3) \quad \frac{\partial c_v^*}{\partial t^*} = \alpha^* \phi_v^{*\frac{1}{3}} D_v \frac{6}{k_{sv2} l_l} (c_h^* - c_v^*) + \gamma^* \phi_v^{*-1} \frac{12 \phi_{cd} D_v}{m^2} (c_{\text{sat}} - c_v^*) \psi_v^*$$

$$(2.4) \quad -\frac{c_v^*}{\phi_v^*} \frac{\partial \phi_v^*}{\partial t^*},$$

$$\frac{\partial \phi_v^*}{\partial t^*} = -\frac{1}{r_s} \frac{\partial \psi_s^*}{\partial t^*} - \frac{1}{r_v} \frac{\partial \psi_v^*}{\partial t^*},$$

$$(2.5) \quad \frac{\partial \psi_s^*}{\partial t^*} = -\beta^* \frac{12D_h \phi_{cd}}{k_{sv1} m} \left(\frac{c_{\text{sat}} - c_h^*}{c_s} \right) r_s \psi_s^*,$$

$$(2.6) \quad \frac{\partial \psi_v^*}{\partial t^*} = -\gamma^* \frac{12D_v \phi_{cd}}{m^2} \left(\frac{c_{\text{sat}} - c_v^*}{c_s} \right) r_v \psi_v^*.$$

$$(2.7) \quad 0 < z^* < L, \quad t^* > 0,$$

$$(2.8) \quad c_h^*(z^*, 0) = c_{h0}^*(z^*), \quad c_v^*(z^*, 0) = c_{v0}^*(z^*),$$

$$\phi_v^*(z^*, 0) = \phi_{v0}^*(z^*), \quad \psi_s^*(z^*, 0) = \psi_{s0}^*(z^*), \quad \psi_v^*(z^*, 0) = \psi_{v0}^*(z^*),$$

$$(2.9) \quad p_h^*(0, t^*) = 0, \quad p_h^*(L, t^*) = \Delta P, \quad c_h^*(L, t^*) = 0, \quad \frac{\partial c_h^*(0, t^*)}{\partial z^*} = 0.$$

Here r_s and r_v are the reciprocals of $\phi_{s,sd}$ and $\phi_{s,bd}$, respectively. The pressure boundary conditions come from the recorded pressure drop in experiment. The concentration in the incoming water is zero at the inlet, and it is assumed that the diffusive flux is zero at the outlet. Initial conditions need to be determined or inferred from experiment once the bed is saturated with water, following the initial addition of water to the dry coffee bed. The initial conditions could also be determined by modeling the unsaturated flow during the initial infiltration of water. Note the presence of experimental fitting parameters, α^* , β^* , and γ^* , for the mass transfer terms. These parameters are used to fit the model to the experiment. These are required because many of the parameters in the model are difficult to obtain. For example, the diffusion coefficient used here will be for caffeine in water. This value may not be reflective of the effective diffusivity of coffee solubles in the system. Other parameters such as the average diffusion distance l_l , average cell radius m , and the specific surface areas are similarly difficult to estimate accurately. Thus fitting parameters are required to account for errors in each of the components of their respective mass transfer coefficients.

The full description and derivation of (2.1)–(2.6) are contained in [14]. Here it will suffice to outline the meaning of the equations in the context of Figure 2. Equation (2.1) tracks concentration of coffee in the intergranular pores. The first term on the right-hand side of the equation represents advection of coffee in the fluid in the bed, described using Darcy's law and the Kozeny–Carman equations. The second and third terms represent diffusion and mechanical dispersion of coffee in the flow. The fourth term represents transfer of coffee from the intact cells in the grain kernels (intragranular pores) to the intergranular pores via slow diffusion through the tortuous grains. The final term represents fast release of coffee from the broken cells in the fine grains and the grain surfaces. Equation (2.2) gives the flow equation for the fluid in the intergranular pores according to Darcy's law. Equation (2.3) tracks the concentration of coffee solubles in the intragranular pores. Note here that the intragranular porosity, ϕ_v^* , changes as coffee dissolves in the grains. The quantity of coffee in the intragranular pores is reduced by slow diffusion to the intergranular pores (first term) and increased by coffee dissolving from the cell walls in the grain kernels

(second term). The final term is a volume correction to account for the changing porosity. Equations (2.5) and (2.6) track the fraction of the initial amount of coffee (in dry grains) remaining on the grain surfaces and in the solid matrix in the grain kernels, respectively. As coffee dissolves, the intragranular porosity increases, and this increase is tracked in (2.4). In the following section, this dimensional system of equations will be specialized to model experimental results for extraction of coffee from a packed coffee bed. The model will be nondimensionalized, and the dominant terms will be analyzed to develop approximate solutions.

2.3. Modeling assumptions. Before nondimensionalizing the system, we can take some further simplifying steps. Equation (2.2) can be solved using the pressure boundary conditions from the experiment in question to find $p_h^* = \frac{\Delta P}{L} z^*$. Substituting this into (2.1) eliminates p_h^* . Integrating (2.4) with respect to time, we see that

$$(2.10) \quad \phi_v^* + \frac{1}{r_s} \psi_s^* + \frac{1}{r_v} \psi_v^* = f(z),$$

where $f(z)$ is an arbitrary function of z . We note that this is just the sum of the intragranular pore volume fraction, the volume fraction of solid coffee on the surface, and the volume fraction of solid coffee in the grain kernels. This sum must be equal to the maximum intragranular pore volume fraction (porosity), which we define as ϕ_v^∞ , and corresponds to the situation in which all soluble coffee is dissolved. The value of ϕ_v^∞ can be estimated from data on the percentage of the coffee grain mass which is soluble for a given coffee grind. Thus we can eliminate ϕ_v^* from the system using (2.4) and

$$(2.11) \quad \phi_v^* = \phi_v^\infty - \frac{1}{r_s} \psi_s^* - \frac{1}{r_v} \psi_v^*.$$

However, this still leaves us with quite a complex system to analyze. To further simplify, we assume that the volume fraction of coffee in the grains is small compared to the final intragranular porosity. This corresponds to $\phi_{s,sd} + \phi_{s,bd} = r_s^{-1} + r_v^{-1} \ll \phi_v^\infty$. Thus we make the approximation that $\phi_v^* \approx \phi_v^\infty$ in the equations. We need to account for this when assigning initial conditions in the intragranular pores.

In order to use the model, we need to find values for α^* , β^* , and γ^* . Experimental extraction profiles are available for c_h^* at the filter exit, and the two rates of extraction are evident in the profiles. Thus α^* and β^* can be fitted. Data is not available for c_v^* , however, so γ^* cannot be determined. A reasonable approximation may be that $\gamma^* \approx \beta^*$. In reality, due to a much larger surface area per unit volume within the grains, it is likely that $\gamma^* > \beta^*$. Dissolution of coffee within the coffee grain and diffusion of coffee from the grain pore network occur consecutively. Based on the assumption that $\gamma^* \geq \beta^*$, the diffusion of coffee is the rate limiting step in this series. We expect dissolution within the grains to proceed at a rate similar to that of dissolution from grain surfaces, but experiments show a much slower extraction from the grains, so the diffusion limited assumption seems reasonable. Thus, to simplify the analysis, we assume the solid coffee in the cell walls within the grains dissolves into the intragranular pores very quickly initially so that all soluble coffee in the grains is dissolved in the fluid in the intragranular pores initially (i.e., once the coffee bed is saturated with water). The validity of this assumption is based on the timescale of the dissolution process being much shorter than the grain diffusion timescale. Provided that diffusion of coffee from the grains is the rate limiting step of extraction, rather than solid dissolution within the grains, the model may still work quite well. This

corresponds to $\psi_v^*(z^*, 0) = 0$ and means (2.6) drops out. This also allows us to estimate $c_v^*(z^*, 0)$ by assuming all the soluble coffee in the grain kernels has dissolved in the intragranular pores. Thus we let $c_v^*(z^*, 0) = \eta c_{\text{sat}}$ with $0 \leq \eta \leq 1$ depending on the coffee grind in question. The unsaturated flow during the initial infiltration of water into the dry bed is not modeled here. This means we need to estimate the remaining initial conditions after the bed is saturated with water and coffee brew starts to exit at the bottom. Experiments suggest that the exiting coffee concentration may be steady for perhaps the first wash through of the coffee bed before it starts to drop. Initial exiting concentration for fine grinds is significantly higher than for coarser grinds and may be close to the solubility of coffee in water. Based on the experiment data it will be assumed that the initial concentration profile for the fine grind considered is at coffee solubility throughout the bed, so $c_h^*(z^*, 0) = c_{\text{sat}}$. For coarser grinds a linear initial coffee concentration profile will be assumed varying from 0 at the filter entrance to the initial exiting concentration from experiments c_{max} at the filter exit. So, for coarser grinds, $c_h^*(z^*, 0) = c_{\text{max}} \frac{(L-z^*)}{L}$. More generally it would be useful to find approximate solutions for an initial concentration profile which is an arbitrary function of z^* . It remains to assign the initial condition to $\psi_s^*(z^*, 0)$, which represents the fraction of the initial volume fraction of soluble coffee on the grain surfaces remaining following water infiltration. One would expect this term to be smaller at the top of the bed than at the bottom since water is in contact with these grinds longer during infiltration. However, without modeling the initial water infiltration, the simplest assumption is to uniformly decrease $\psi_s^*(z^*, 0)$ to correspond to the amount of coffee which has dissolved to give $c_h^*(z^*, 0)$. Thus we let $\psi_s^*(z^*, 0) = \psi_{s0}^*$ with $0 \leq \psi_{s0}^* \leq 1$. ψ_{s0}^* depends on the parameters of the coffee grind in question and the assumed initial concentration profile. With all this in mind, we rewrite the dimensional equations for the fine grind coffee as

$$(2.12) \quad \begin{aligned} \frac{\partial c_h^*}{\partial t^*} &= \frac{k_{sv1}^2 \phi_h^2}{36\kappa\mu(1-\phi_h)^2} \left(\frac{\Delta P}{L} + \rho g \right) \frac{\partial c_h^*}{\partial z^*} + \phi_h^{\frac{1}{3}} D_h \frac{\partial^2 c_h^*}{\partial z^{*2}} \\ &+ D^b \frac{\partial^2 c_h^*}{\partial z^{*2}} - \alpha^* \frac{(1-\phi_h)}{\phi_h} \phi_v^{\infty \frac{4}{3}} D_v \frac{6}{k_{sv2} l} (c_h^* - c_v^*) \\ &+ \beta^* \frac{(1-\phi_h)}{\phi_h} \frac{12D_h \phi_{cd}}{k_{sv1} m} (c_{\text{sat}} - c_h^*) \psi_s^*, \end{aligned}$$

$$(2.13) \quad \frac{\partial c_v^*}{\partial t^*} = \alpha^* \phi_v^{\infty \frac{1}{3}} D_v \frac{6}{k_{sv2} l} (c_h^* - c_v^*),$$

$$(2.14) \quad \frac{\partial \psi_s^*}{\partial t^*} = -\beta^* \frac{12D_h \phi_{cd}}{k_{sv1} m} \left(\frac{c_{\text{sat}} - c_h^*}{c_s} \right) r_s \psi_s^*,$$

$$(2.15) \quad 0 < z^* < L, \quad t^* > 0,$$

$$(2.16) \quad c_h^*(z^*, 0) = c_{\text{sat}}, \quad c_v^*(z^*, 0) = \eta c_{\text{sat}}, \quad \psi_s^*(z^*, 0) = \psi_{s0}^*,$$

$$(2.17) \quad c_h^*(L, t^*) = 0, \quad \frac{\partial c_h^*(0, t^*)}{\partial z^*} = 0.$$

We also have $\psi_v^*(z^*, t^*) = 0$, and $\phi_v^*(z^*, t^*)$ is given by (2.11). A summary of the model parameters and values is given in Table 1. Note that the solution here will be

based on the assumed initial conditions for a fine coffee grind as outlined above. Once the initial conditions are changed, the solution for the coarse grind follows the same steps.

TABLE 1
Parameters for cylindrical brewing chamber extraction experiments [14].

Parameter	Description	Value
ϕ_v^∞	intragranular porosity	0.7034
ϕ_h	intergranular porosity	0.2
c_s	coffee solid density	1400 kg m ⁻³
ϕ_{cd}	soluble coffee volume fraction	0.143435
$\phi_{s,sd}$	surface coffee volume fraction	0.11
$\phi_{s,bd}$	grain kernel coffee volume fraction	0.033435
α^*	grain diffusion fitting coefficient	0.1833
β^*	surface dissolution fitting coefficient	0.0447
ΔP	pressure drop across bed	230 000 Pa
L	coffee bed height	0.0405 m
k_{sv1}	Sauter mean diameter (all grains)	27.35 μm
k_{sv2}	Sauter mean diameter (grains > 50 μm)	322.49 μm
l_l	mean volume weighted grain radius	282 μm
$D_h = D_v$	coffee diffusion coefficient (for caffeine [12])	2.2×10^{-9} m ² s ⁻¹
ρ	liquid density (for water at 90 °C)	965.3 kg m ⁻³
μ	liquid viscosity (for water at 90 °C)	0.315×10^{-3} Pa s
m	coffee cell diameter	30 μm
c_{sat}	coffee solubility	212.4 kg m ⁻³
κ	Kozeny–Carman shape coefficient	3.1
η	initial intragranular concentration level	0.5
ψ_{s0}^*	fraction of $\phi_{s,sd}$ remaining after filling	0.7304
g	acceleration due to gravity	9.81 m s ⁻²

2.4. Nondimensionalization. For the parameters involved in the extraction experiments for either the coarse or fine coffee grinds, the advection term is found to dominate strongly over the diffusion and mechanical dispersion terms in (2.12). To see this we consider the ratio of the advection term to the diffusion term (with $z^* \sim L$) for the coffee flow-through cell which is given by

$$(2.18) \quad \frac{k_{sv1}^2 L \phi_h^{\frac{5}{3}}}{36 \kappa \mu D_h (1 - \phi_h)^2} \left(\frac{\Delta P}{L} + \rho g \right).$$

For the experiments in question here we have $\frac{\Delta P}{L} \gg \rho g$, so the ratio is approximately given by

$$(2.19) \quad \frac{k_{sv1}^2 \Delta P \phi_h^{\frac{5}{3}}}{36 \kappa \mu D_h (1 - \phi_h)^2}.$$

We use the parameters from Table 1 to estimate this term. Thus

$$(2.20) \quad \frac{k_{sv1}^2 \Delta P \phi_h^{\frac{5}{3}}}{36 \kappa \mu D_h (1 - \phi_h)^2} \sim 10^7,$$

and so advection dominates strongly over diffusion. Similarly, the ratio of advection to dispersion is

$$(2.21) \quad \frac{k_{sv1}^2 L \phi_h^2}{36 \kappa \mu D^b (1 - \phi_h)^2} \left(\frac{\Delta P}{L} + \rho g \right) \approx \frac{k_{sv1}^2 \Delta P \phi_h^2}{36 \kappa \mu D^b (1 - \phi_h)^2}.$$

The dispersion coefficient is more difficult to estimate and is related to the pore size and the fluid velocity in the pores. In [14] a general expression for the dispersion coefficient in terms of fluid velocity and average pore size is used to show the dominance of advection. Here we just note that unless the dispersion coefficient is many orders of magnitude greater in size than the diffusion coefficient, advection dominates over dispersion. For this reason these terms are neglected.

There are three main timescales of interest in the model. The timescale over which coffee diffuses from the grain kernels to the intergranular pores is referred to as the bulk diffusion timescale t_d . The timescale over which the coffee dissolves from the grain surfaces into the intergranular pores is referred to as the surface dissolution timescale t_s . Finally, the timescale over which the coffee solubles are carried in the flow out of the bed is referred to as the advection timescale t_a . In terms of the coffee bed parameters, these timescales are defined as

$$(2.22) \quad t_d = \frac{k_{sv2}l_l}{6\alpha^*\phi_v^{\infty\frac{1}{3}}D_v}, \quad t_s = \frac{k_{sv1}m\phi_h}{12\beta^*D_h\phi_{cd}\psi_{s0}^*(1-\phi_h)}, \quad t_a = \frac{36L^2\kappa\mu(1-\phi_h)^2}{k_{sv1}^2\phi_h^2(\Delta P + \rho gL)}.$$

For the fine grind parameters from [14], $t_s = 1.042$ s, $t_a = 5.356$ s, and $t_d = 42.231$ s. First we scale the equations on the bulk diffusion timescale. The concentration scale for the intergranular pores is chosen to balance the advection term with the transfer of coffee solubles by diffusion from the grains. The scale for the ψ_s^* is chosen so that the source term for transfer of coffee from the surface balances the previous two terms. The scales chosen are as follows:

$$(2.23) \quad c_h^* \sim \frac{216\kappa\mu L^2\alpha^*D_v\phi_v^{\infty\frac{4}{3}}(1-\phi_h)^3}{k_{sv2}k_{sv1}^2\phi_h^3l_l(\Delta P + \rho gL)}c_{\text{sat}}, \quad c_v^* \sim c_{\text{sat}}, \quad t^* \sim t_d = \frac{k_{sv2}l_l}{6\alpha^*\phi_v^{\infty\frac{1}{3}}D_v},$$

$$(2.24) \quad \psi_s^* \sim \frac{\alpha^*D_v\phi_v^{\infty\frac{4}{3}}k_{sv1}m}{2\beta^*D_h\phi_{cd}k_{sv2}l_l}, \quad z^* \sim L.$$

Before we present the nondimensional equations on the bulk diffusion timescale, we define some nondimensional parameters to tidy up the presentation. First we define ϵ to be the ratio of the advection timescale to the timescale of diffusion of coffee from the grains. Thus

$$(2.25) \quad \epsilon = \frac{216\kappa\mu L^2\alpha^*D_v\phi_v^{\infty\frac{1}{3}}(1-\phi_h)^2}{k_{sv2}k_{sv1}^2\phi_h^2l_l(\Delta P + \rho gL)} = \frac{t_a}{t_d}.$$

The other three nondimensional parameters are given by

$$(2.26) \quad a_1 = \frac{1-\phi_h}{\phi_h}\phi_v^{\infty}, \quad a_2 = \frac{432\kappa\mu L^2\beta^*D_h\phi_{cd}\psi_{s0}^*(1-\phi_h)^3}{k_{sv1}^3m\phi_h^3(\Delta P + \rho gL)} = \frac{t_a}{t_s}, \quad a_3 = \frac{c_{\text{sat}}r_s\phi_h}{c_s(1-\phi_h)\psi_{s0}^*}.$$

Physically a_1 represents the ratio of the intragranular volume to the intergranular volume, a_2 represents the ratio of the advection timescale to the surface dissolution timescale, and a_3 represents the ratio of the maximum coffee mass capacity of the intergranular pores to the initial mass of coffee present on the grain surfaces. We will assume here that $\epsilon \ll 1$, while a_1 , a_2 , and a_3 are all $O(1)$. For the fine grind parameters we have $\epsilon = 0.127$, $a_1 = 2.81$, $a_2 = 5.139$, and $a_3 = 0.473$. In terms of these parameters, the equations on the bulk diffusion timescale with boundary and initial conditions prescribed are

$$(2.27) \quad \epsilon \frac{\partial C_h}{\partial \tau} = \frac{\partial C_h}{\partial z} - \epsilon a_1 C_h + C_v + (1 - a_1 \epsilon C_h) \Psi_s,$$

$$(2.28) \quad \frac{\partial C_v}{\partial \tau} = a_1 \epsilon C_h - C_v,$$

$$(2.29) \quad \epsilon \frac{\partial \Psi_s}{\partial \tau} = -a_2 a_3 (1 - a_1 \epsilon C_h) \Psi_s,$$

$$(2.30) \quad 0 < z < 1, \quad \tau > 0,$$

$$(2.31) \quad C_h(z, 0) = \frac{1}{a_1 \epsilon}, \quad C_v(z, 0) = \eta,$$

$$(2.32) \quad \Psi_s(z, 0) = \frac{a_2 \psi_{s0}^*}{a_1 \epsilon}, \quad C_h(1, \tau) = 0.$$

It is clear from the form of the equations that we have a singular perturbation problem. Thus we will need to consider the dynamics of the system on an initial layer in order to satisfy the initial conditions. First we will solve the outer equations using a regular expansion. Any constants of integration which arise will need to be matched to the initial layer solutions when they are found.

3. Asymptotic solutions.

3.1. Perturbation solutions on the bulk diffusion (outer) timescale. We use the following expansions for the bulk diffusion timescale:

$$(3.1) \quad C_h \sim C_{h0} + \epsilon C_{h1} + \epsilon^2 C_{h2},$$

$$(3.2) \quad C_v \sim C_{v0} + \epsilon C_{v1} + \epsilon^2 C_{v2},$$

$$(3.3) \quad \Psi_s \sim \Psi_{s0} + \epsilon \Psi_{s1} + \epsilon^2 \Psi_{s2}.$$

3.1.1. Leading order solutions. The leading order equations are

$$(3.4) \quad \frac{\partial C_{h0}}{\partial z} = -C_{v0} - \Psi_{s0},$$

$$(3.5) \quad \frac{\partial C_{v0}}{\partial \tau} = -C_{v0},$$

$$(3.6) \quad \Psi_{s0} = 0,$$

with solutions

$$(3.7) \quad C_{h0}(z, \tau) = -e^{-\tau} \int_1^z f_1(\xi) d\xi, \quad C_{v0}(z, \tau) = e^{-\tau} f_1(z), \quad \Psi_{s0}(z, \tau) = 0,$$

where $f_1(z)$ is an arbitrary function of z to be determined by matching.

3.1.2. Order ϵ solutions. Substituting in the known terms and using $\Psi_{s1} = 0$ from the third equation in the first and second, the first order equations are

$$(3.8) \quad \frac{\partial C_{h1}}{\partial z} = e^{-\tau} (1 - a_1) \int_1^z f_1(\xi) d\xi - C_{v1},$$

$$(3.9) \quad \frac{\partial C_{v1}}{\partial \tau} = -C_{v1} - a_1 e^{-\tau} \int_1^z f_1(\xi) d\xi,$$

$$(3.10) \quad \Psi_{s1} = 0,$$

with solutions

$$(3.11) \quad C_{h1}(z, \tau) = -e^{-\tau} \left(\int_1^z f_2(\xi) d\xi \right) - e^{-\tau} (a_1\tau - a_1 + 1) \left(\int_1^z \int_1^\lambda f_1(\xi) d\xi d\lambda \right),$$

$$(3.12) \quad C_{v1}(z, \tau) = e^{-\tau} f_2(z) - a_1 e^{-\tau} \tau \left(\int_1^z f_1(\xi) d\xi \right),$$

$$(3.13) \quad \Psi_{s1}(z, \tau) = 0,$$

where $f_2(z)$ is a second arbitrary function of z to be determined by matching.

3.1.3. Solutions for the bulk diffusion (outer) timescale. In summary, we have the following outer solutions:

$$(3.14) \quad C_h(z, \tau) = -e^{-\tau} \int_1^z f_1(\xi) d\xi \\ - \epsilon \left(e^{-\tau} \left(\int_1^z f_2(\xi) d\xi \right) \right) \\ - \epsilon \left(e^{-\tau} (a_1\tau - a_1 + 1) \left(\int_1^z \int_1^\lambda f_1(\xi) d\xi d\lambda \right) \right),$$

$$(3.15) \quad C_v(z, \tau) = e^{-\tau} f_1(z) \\ + \epsilon \left(e^{-\tau} f_2(z) - a_1 e^{-\tau} \tau \left(\int_1^z f_1(\xi) d\xi \right) \right),$$

$$(3.16) \quad \Psi_s(z, \tau) = 0.$$

3.2. Perturbation solutions on the advection (inner) timescale. In this section we will consider the system behavior in the initial layer. We rescale time via $\tau = \epsilon t$. We also rescale c_h^* and ψ_s^* to account for the different balances in the system in the initial layer. In particular, the variables are rescaled as follows:

$$(3.17) \quad \tau = \epsilon t, \quad C_h(z, \tau) = \frac{1}{a_1 \epsilon} c_h(z, t),$$

$$(3.18) \quad C_v(z, \tau) = c_v(z, t), \quad \Psi_s(z, \tau) = \frac{a_2}{a_1 \epsilon} \psi_s(z, t).$$

The scales for each of the dimensional variables in the initial layer are

$$(3.19) \quad c_h^* \sim c_{\text{sat}}, \quad c_v^* \sim c_{\text{sat}}, \quad t^* \sim t_a = \frac{36L^2 \kappa \mu (1 - \phi_h)^2}{k_{sv1}^2 \phi_h^2 (\Delta P + \rho g L)},$$

$$(3.20) \quad z^* \sim L, \quad \psi_s^* \sim \psi_{s0}^*.$$

Thus the equations on the inner timescale are given by

$$(3.21) \quad \frac{\partial c_h}{\partial t} = \frac{\partial c_h}{\partial z} - \epsilon a_1 (c_h - c_v) + a_2 (1 - c_h) \psi_s,$$

$$(3.22) \quad \frac{\partial c_v}{\partial t} = \epsilon (c_h - c_v),$$

$$(3.23) \quad \frac{\partial \psi_s}{\partial t} = -a_2 a_3 (1 - c_h) \psi_s,$$

$$(3.24) \quad 0 < z < 1, \quad t > 0,$$

$$(3.25) \quad c_h(z, 0) = 1, \quad c_v(z, 0) = \eta,$$

$$(3.26) \quad \psi_s(z, 0) = 1, \quad c_h(1, t) = 0.$$

We use the following expansions for the advection timescale:

$$(3.27) \quad c_h \sim c_{h0} + \epsilon c_{h1} + \epsilon^2 c_{h2},$$

$$(3.28) \quad c_v \sim c_{v0} + \epsilon c_{v1} + \epsilon^2 c_{v2},$$

$$(3.29) \quad \psi_s \sim \psi_{s0} + \epsilon \psi_{s1} + \epsilon^2 \psi_{s2}.$$

3.2.1. Leading order equations. The leading order equations are

$$(3.30) \quad \frac{\partial c_{h0}}{\partial t} = \frac{\partial c_{h0}}{\partial z} + a_2(1 - c_{h0})\psi_{s0},$$

$$(3.31) \quad \frac{\partial c_{v0}}{\partial t} = 0,$$

$$(3.32) \quad \frac{\partial \psi_{s0}}{\partial t} = -a_2 a_3 (1 - c_{h0})\psi_{s0},$$

$$(3.33) \quad 0 < z < 1, \quad t > 0,$$

$$(3.34) \quad c_{h0}(z, 0) = 1, \quad c_{v0}(z, 0) = \eta,$$

$$(3.35) \quad \psi_{s0}(z, 0) = 1, \quad c_{h0}(1, t) = 0.$$

Integrating (3.31) and applying the initial condition gives $c_{v0}(z, t) = \eta$. Next we solve (3.32) for c_{h0} to get

$$(3.36) \quad c_{h0} = 1 + \frac{1}{a_2 a_3 \psi_{s0}} \frac{\partial \psi_{s0}}{\partial t} = 1 + \frac{1}{a_2 a_3} \frac{\partial (\ln \psi_{s0})}{\partial t}.$$

Now, substituting this into (3.30) and simplifying gives

$$(3.37) \quad \frac{\partial^2 (\ln \psi_{s0})}{\partial t^2} = \frac{\partial^2 (\ln \psi_{s0})}{\partial t \partial z} - a_2 \frac{\partial \psi_{s0}}{\partial t}.$$

Integrating this with respect to time gives

$$(3.38) \quad \frac{\partial (\ln \psi_{s0})}{\partial t} = \frac{\partial (\ln \psi_{s0})}{\partial z} - a_2 \psi_{s0} + g_1(z),$$

where $g_1(z)$ is the constant of integration. Thus we have

$$(3.39) \quad \frac{\partial \psi_{s0}}{\partial t} = \frac{\partial \psi_{s0}}{\partial z} - a_2 \psi_{s0}^2 + g_1(z) \psi_{s0}.$$

Using the initial condition $\psi_{s0}(z, 0) = 1$ and noting that since $c_{h0}(z, 0) = 1$ then $\frac{\partial \psi_{s0}}{\partial t}(z, 0) = 0$, we see that $g_1(z) = a_2$. Also, since $c_{h0}(1, t) = 0$, it is easily found that $\psi_{s0}(1, t) = \exp(-a_2 a_3 t)$. Thus the leading order problem for ψ_{s0} is

$$(3.40) \quad \frac{\partial \psi_{s0}}{\partial t} = \frac{\partial \psi_{s0}}{\partial z} - a_2 \psi_{s0}^2 + a_2 \psi_{s0},$$

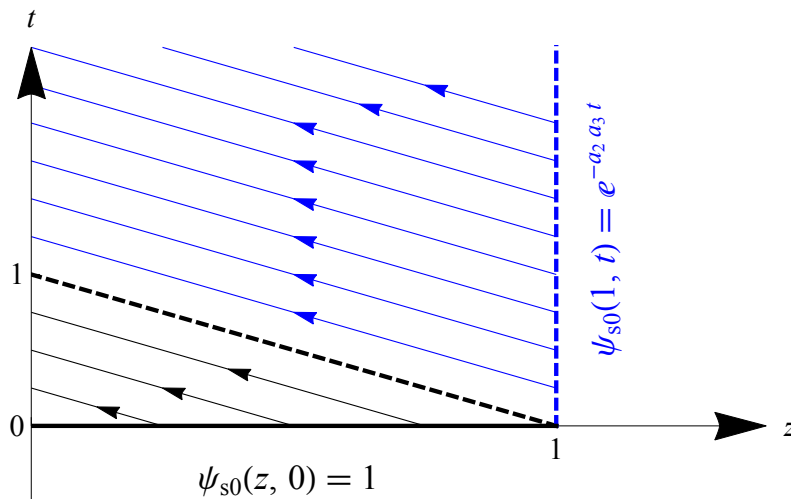


FIG. 4. Characteristic curves $z + t = c$ of (3.42). Note that the solution propagates from the initial condition for $z + t < 1$, while it propagates from the boundary condition for $z + t > 1$.

$$(3.41) \quad \psi_{s0}(z, 0) = 1, \quad \psi_{s0}(1, t) = e^{-a_2 a_3 t}.$$

We can rewrite this as

$$(3.42) \quad \frac{\partial \psi_{s0}}{\partial t} - \frac{\partial \psi_{s0}}{\partial z} = -a_2 \psi_{s0} (1 - \psi_{s0}),$$

which we can solve using the method of characteristics. We have

$$(3.43) \quad \frac{d\psi_{s0}}{dt} = -a_2 \psi_{s0} (1 - \psi_{s0}) \quad \text{on} \quad \frac{dz}{dt} = -1.$$

If ψ_{s0} is 0 or 1, it remains so; otherwise we solve the equation along the characteristics $z + t = c$, c constant. The characteristics are shown in Figure 4. We note that the solution propagates from the initial condition at $t = 0$ for $z + t < 1$, while it propagates from the boundary condition at $z = 1$ for $z + t > 1$. In this case, since the initial condition is $\psi_{s0}(z, 0) = 1$, we have $\psi_{s0} = 1$ for all $z + t < 1$. We solve the equations above for $z + t > 1$ to get

$$(3.44) \quad \psi_{s0}(z, t) = \begin{cases} 1, & z + t < 1, \\ \frac{e^{a_2}}{e^{a_2 - e^{a_2} z} + e^{a_2(z + a_3(z + t - 1))}}, & z + t > 1. \end{cases}$$

This also gives us the leading order solution for c_{h0} :

$$(3.45) \quad c_{h0}(z, t) = \begin{cases} 1, & z + t < 1, \\ \frac{e^{a_2} - e^{a_2 z}}{e^{a_2 - e^{a_2} z} + e^{a_2(z + a_3(z + t - 1))}}, & z + t > 1. \end{cases}$$

3.2.2. Order ϵ equations. The order ϵ equations are

$$(3.46) \quad \frac{\partial c_{h1}}{\partial t} = \frac{\partial c_{h1}}{\partial z} + a_2(1 - c_{h0})\psi_{s1} - a_1(c_{h0} - c_{v0}) - a_2 c_{h1} \psi_{s0},$$

$$(3.47) \quad \frac{\partial c_{v1}}{\partial t} = c_{h0} - c_{v0},$$

$$(3.48) \quad \frac{\partial \psi_{s1}}{\partial t} = -a_2 a_3 (1 - c_{h0}) \psi_{s1} + a_2 a_3 c_{h1} \psi_{s0},$$

$$(3.49) \quad 0 < z < 1, \quad t > 0,$$

$$(3.50) \quad c_{h1}(z, 0) = 0, \quad c_{v1}(z, 0) = 0,$$

$$(3.51) \quad \psi_{s1}(z, 0) = 0, \quad c_{h1}(1, t) = 0.$$

First we solve (3.47). We substitute the known values in for c_{h0} and c_{v0} . As c_{h0} is different for $z + t < 1$ and $z + t > 1$, so is c_{v1} . Solving the equations, we find that

$$(3.52) \quad c_{v1}(z, t) = \begin{cases} (1 - \eta)t, & z + t < 1, \\ (1 - \eta)t + \frac{1}{a_2 a_3} \ln \left(\frac{e^{a_2}}{e^{a_2 - e^{a_2 z} + e^{a_2(z+a_3(z+t-1))}}}, \right) & z + t > 1. \end{cases}$$

Next we solve (3.48) for c_{h1} in terms of ψ_{s1} . We can do this for $z + t < 1$ and $z + t > 1$, but only the former yields a solution for ψ_{s1} and c_{h1} , and so only this is presented here. For $z + t < 1$ we get

$$(3.53) \quad c_{h1} = \frac{1}{a_2 a_3} \frac{\partial \psi_{s1}}{\partial t}.$$

As was done at leading order, we can substitute this into (3.46), integrate with respect to time, and use initial conditions to evaluate the constant of integration. This leads to the equation

$$(3.54) \quad \frac{\partial \psi_{s1}}{\partial t} - \frac{\partial \psi_{s1}}{\partial z} = -a_2 \psi_{s1} - \eta a_1 a_2 a_3 t.$$

Again, this can be solved by the method of characteristics so that for $z + t < 1$ we have

$$(3.55) \quad \psi_{s1}(z, t) = \frac{a_1 a_3 ((\eta - 1)e^{-a_2 t} (1 + e^{a_2 t} (a_2 t - 1)))}{a_2}.$$

This also gives us c_{h1} for $z + t < 1$:

$$(3.56) \quad c_{h1}(z, t) = \frac{a_1 (\eta - 1) e^{-a_2 t} (e^{a_2 t} - 1)}{a_2}.$$

The same steps can be tried for $z + t > 1$; however, the integration with respect to time is not possible in this case.

3.2.3. Solutions on the advection (inner) timescale. In summary, we have the following inner solutions:

$$(3.57) \quad c_h(z, t) = \begin{cases} 1 + \epsilon \left(\frac{a_1 (\eta - 1) e^{-a_2 t} (e^{a_2 t} - 1)}{a_2} \right), & z + t < 1, \\ \frac{e^{a_2} - e^{a_2 z}}{e^{a_2 - e^{a_2 z} + e^{a_2(z+a_3(z+t-1))}}}, & z + t > 1, \end{cases}$$

$$(3.58) \quad c_v(z, t) = \begin{cases} \eta + \epsilon ((1 - \eta)t), & z + t < 1, \\ \eta + \epsilon \left((1 - \eta)t + \frac{1}{a_2 a_3} \ln \left(\frac{e^{a_2}}{e^{a_2 - e^{a_2 z} + e^{a_2(z+a_3(z+t-1))}}}, \right) \right), & z + t > 1, \end{cases}$$

$$(3.59) \quad \psi_s(z, t) = \begin{cases} 1 + \epsilon \left(\frac{a_1 a_3 ((\eta - 1) e^{-a_2 t} (1 + e^{a_2 t} (a_2 t - 1)))}{a_2} \right), & z + t < 1, \\ \frac{e^{a_2}}{e^{a_2 - e^{a_2 z} + e^{a_2(z+a_3(z+t-1))}}}, & z + t > 1. \end{cases}$$

3.3. Matching. We can find the constants of integration remaining in the outer solution by using modified Van Dyke matching [23] to match the initial layer solution with the outer solution. This method involves comparing the inner expansion of the outer solutions with the outer expansion of the inner (initial layer) solutions to obtain unknown functions $f_1(z)$ and $f_2(z)$ in (3.14) and (3.15). This yields

$$(3.60) \quad f_1(z) = \eta, \quad f_2(z) = \left(\frac{1}{a_3} + 1\right)(1 - z).$$

Thus the outer solutions are

$$(3.61) \quad C_h(z, \tau) = e^{-\tau}(\eta - \eta z) + \epsilon \left(\frac{1}{2a_3} e^{-\tau} ((z-1)^2(1 + a_3(1 + \eta(1 + a_1(\tau - 1)))) \right),$$

$$(3.62) \quad C_v(z, \tau) = \eta e^{-\tau} + \epsilon \left(-e^{-\tau}(-\eta a_1 + \eta a_1 z)\tau + e^{-\tau} \left(\left(\frac{1}{a_3} + 1 \right) (1 - z) \right) \right),$$

$$(3.63) \quad \Psi_s(z, \tau) = 0.$$

3.4. Composite solutions. We have inner and outer solutions for our equations. For c_h we obtain an expansion to leading order in the inner layer and to $O(\epsilon)$ in the outer region. The solution for c_v is known to $O(\epsilon)$ in both regions, while ψ_s has an inner solution at leading order while the outer solution is 0 to $O(\epsilon)$. Comparison with numerics shows that the inner and outer solutions fit quite well in their regions of validity. In terms of the initial layer scalings, the outer solution for c_h is zero at leading order. As the initial layer solution can only be determined at leading order, the inner and outer solutions for c_h have no common part. Thus the composite solution is just their sum. The solution for c_v was formed by matching, so we can easily identify the common part and subtract it off. The composite solution for ψ_s is just the inner solution. In terms of the inner scalings and the Heaviside or unit step function $\mathcal{H}(x)$, the composite solutions are

$$(3.64) \quad c_h(z, t) = \left(1 + \epsilon \left(\frac{a_1 e^{-a_2 t} (\eta - 1) (e^{a_2 t} - 1)}{a_2} \right) \right) \mathcal{H}(1 - (z + t)) + \left(\frac{e^{a_2} - e^{a_2 z}}{e^{a_2} - e^{a_2 z} + e^{a_2(z + a_3(z + t - 1))}} \right) \mathcal{H}((z + t) - 1) + \epsilon a_1 \left(e^{-\epsilon t} (\eta - \eta z) + \epsilon \left(\frac{1}{2a_3} e^{-\epsilon t} ((z-1)^2(1 + a_3(1 + \eta(1 + a_1(\epsilon t - 1)))) \right) \right),$$

$$(3.65) \quad c_v(z, t) = (\eta + \epsilon((1 - \eta)t)) \mathcal{H}(1 - (z + t)) + \left(\eta + \epsilon \left((1 - \eta)t + \frac{1}{a_2 a_3} \ln \left(\frac{e^{a_2}}{e^{a_2} - e^{a_2 z} + e^{a_2(z + a_3(z + t - 1))}} \right) \right) \right) \mathcal{H}((z + t) - 1) + \eta e^{-\epsilon t} + \epsilon \left(-e^{-\epsilon t} (-\eta a_1 + \eta a_1 z) \epsilon t + e^{-\epsilon t} \left(\left(\frac{1}{a_3} + 1 \right) (1 - z) \right) \right)$$

$$\begin{aligned}
 & - \left(\eta - \eta \epsilon t + \epsilon \left(\frac{1}{a_3} + 1 \right) (1 - z) \right), \\
 (3.66) \quad \psi_s(z, t) &= \left(1 + \epsilon \left(\frac{a_1 a_3 ((\eta - 1) e^{-a_2 t} (1 + e^{a_2 t} (a_2 t - 1)))}{a_2} \right) \right) \mathcal{H}(1 - (z + t)) \\
 & + \left(\frac{e^{a_2}}{e^{a_2} - e^{a_2 z} + e^{a_2(z + a_3(z + t - 1))}} \right) \mathcal{H}((z + t) - 1),
 \end{aligned}$$

where $\mathcal{H}(x)$ is defined by

$$(3.67) \quad \mathcal{H}(x) = \begin{cases} 1 & \text{if } x \geq 0, \\ 0 & \text{if } x < 0. \end{cases}$$

3.5. Comparison of asymptotics with numerical simulation. Equations (3.21)–(3.26) are solved numerically using the numerical method of lines and compared to the derived composite solutions. The parameters used are those corresponding to JK drip filter grind from [14]. The plots are shown in Figures 5–10. Figure 5 plots the concentration through the bed at different times. At leading order the inner and outer solutions for c_h match identically. As the inner solution could only be determined at leading order and the outer solution is zero at this order, the common part is zero. For this reason the composite solution does not agree well with the numerical solution initially, although inner and outer solutions agree well with the numerical solution over their regions of validity. Figure 6 plots the concentration at the filter exit ($z = 0$) against time. Data points from the experiment (in nondimensional units) are also included for comparison. The inner and outer solutions are plotted separately in the second plot to illustrate their agreement with the numerical solution. The agreement with experimental data shows that the reduced system of equations can still reproduce the experimentally determined extraction profile. Figures 7–10 include the corresponding plots for c_v and ψ_s . Asymptotic solutions are only compared to numerical solutions in this case, due to difficulties in obtaining experimental data for c_v and ψ_s . As was the case with c_h , the disagreement between the asymptotic and numerical solutions for short times with $z + t > 1$ is due to the absence of an order ϵ term in this solution.

4. Conclusion. In this paper we consider some approximate solutions to the coffee extraction model described in [14]. The model equations are simplified and nondimensionalized to describe extraction from a packed coffee bed. Approximate solutions for extraction from a dilute suspension of coffee grains are considered in [15]. The nondimensional equations depend on a small number of parameters and represent a vast simplification of the original equations. We can form approximate solutions to these equations using perturbation techniques. The nondimensional parameters are directly related to the physical parameters of extraction, so these solutions are useful in investigating how a particular parameter affects the extraction profile.

Approximate solutions are formed for the model equations which describe coffee extraction from a packed bed by a pressure driven flow of hot water. The solutions are based on the presence of a small parameter in the system. The small parameter used is the ratio of the advective timescale to the grain diffusion timescale. The initial conditions also need to be estimated here. Different initial conditions are prescribed depending on whether a coarse or fine coffee grind is used, thus leading to different approximate solutions in these situations. The solution for the fine grind

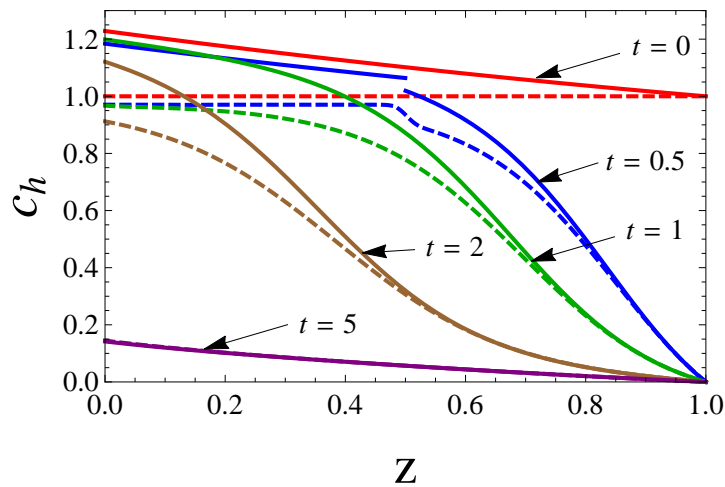


FIG. 5. Plot of numerical (--) and composite (—) solutions with $\epsilon = 0.127$, $a_1 = 2.81$, $a_2 = 5.139$, $a_3 = 0.473$, $\eta = 0.5$ (JK drip filter grind) of c_h versus z at $t = 0$, $t = 0.5$, $t = 1$, $t = 2$, and $t = 5$.

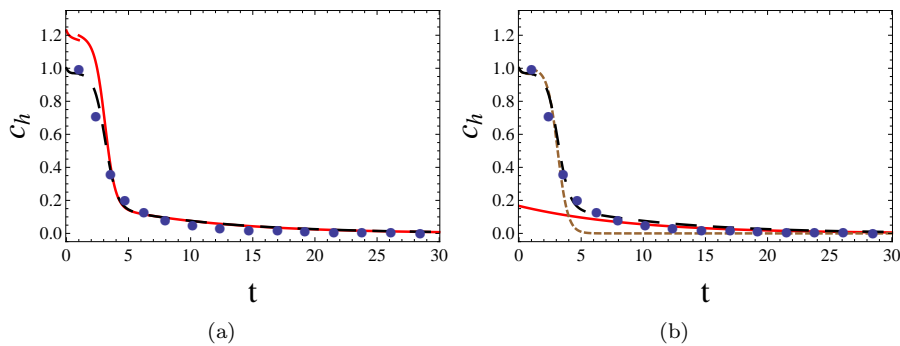


FIG. 6. Plot of numerical (--) and composite (—) solutions with $\epsilon = 0.127$, $a_1 = 2.81$, $a_2 = 5.139$, $a_3 = 0.473$, $\eta = 0.5$ (JK drip filter grind) of (a) c_h versus t at $z = 0$. Experimental data points are included. (b) Plot of numerical solution (—) and inner (--) and outer (—) solutions of c_h versus t at $z = 0$. Experimental data points are included.

case is presented here. Similar solutions can be found for initial conditions in the coarse grind case. Approximate solutions are formed and compared to the numerical solution of the equations and the available experimental data. These solutions allow the coffee quality (in terms of brew strength and extraction yield) at a given time to be explicitly written in terms of the process parameters of the system by integrating the exiting concentration. Such solutions have the potential to be used to evaluate a particular brewing set-up or investigate the impact of changing certain brewing parameters.

There is large scope for further modeling of extraction from coffee beds. The work here and in [14] focuses on extraction of coffee solubles from dilute suspensions of coffee and from a water saturated, packed coffee bed. The model described in [14] can be extended to describe unsaturated flow during filling and draining of the coffee filter. Of particular importance is determining the conditions under which air pockets

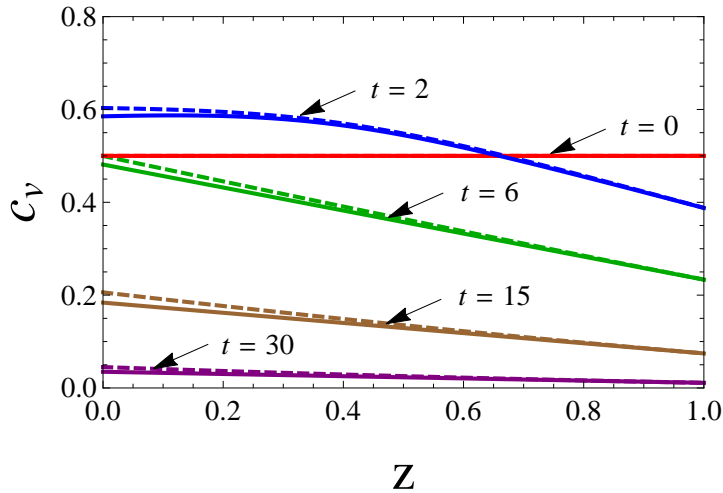


FIG. 7. Plot of numerical (--) and composite (-) solutions with $\epsilon = 0.127$, $a_1 = 2.81$, $a_2 = 5.139$, $a_3 = 0.473$, $\eta = 0.5$ (JK drip filter grind) of c_v versus z at $t = 0$, $t = 2$, $t = 6$, $t = 15$, and $t = 30$.

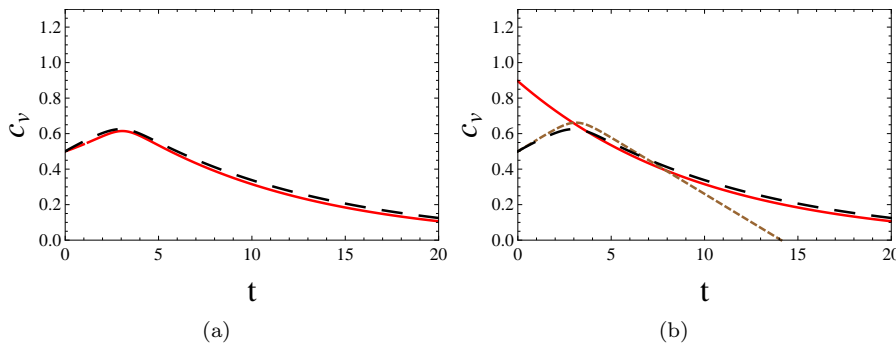


FIG. 8. Plot of numerical (--) and composite (-) solutions with $\epsilon = 0.127$, $a_1 = 2.81$, $a_2 = 5.139$, $a_3 = 0.473$, $\eta = 0.5$ (JK drip filter grind) of (a) c_v versus t at $z = 0$. (b) Plot of numerical (--) and inner (---) and outer (-.-) solutions of c_v versus t at $z = 0$.

can become trapped in the bed during filling, as this leads to an uneven extraction. It is also possible to extend the system of equations to model the extraction of a number of coffee constituents rather than just considering coffee as a single entity. To model a coffee bed in a drip filter machine, one would need to consider a number of further complications. The geometry is different, the flow is more complex, and particles can become entrained in the flow and transported around the bed. The method of delivery of fluid to the bed (single jet or multiple jets) is also important [2]. For fluid delivery with a single jet, the evolution of the coffee bed shape is important, as a central cavity may form in the bed which shortens the path fluid has to travel through the bed to exit the filter. On a smaller scale, there is scope to investigate the kinetics of extraction of coffee on a grain scale and to compare the effectiveness of different kinetic models in describing the extraction.

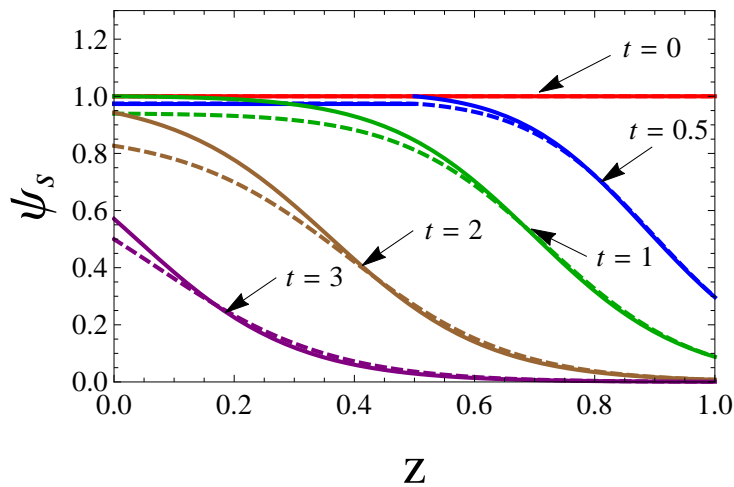


FIG. 9. Plot of numerical (---) and composite (—) solutions with $\epsilon = 0.127$, $a_1 = 2.81$, $a_2 = 5.139$, $a_3 = 0.473$, $\eta = 0.5$ (JK drip filter grind) of ψ_s versus z at $t = 0$, $t = 0.5$, $t = 1$, $t = 2$, and $t = 3$.

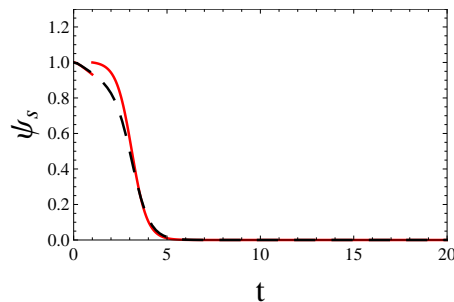


FIG. 10. Plot of numerical (---) and composite (—) solutions with $\epsilon = 0.127$, $a_1 = 2.81$, $a_2 = 5.139$, $a_3 = 0.473$, $\eta = 0.5$ (JK drip filter grind) of ψ_s versus t at $z = 0$.

REFERENCES

- [1] J. BEAR AND A. H.-D. CHENG, *Modeling Groundwater Flow and Contaminant Transport, Theory and Applications of Transport in Porous Media 23*, Springer, Heidelberg, 2010.
- [2] C. BOOTH, C. CUMMINS, M. DALWADI, P. DELLAR, M. DEVEREUX, J. DEWYNNE, J. DONOHUE, A. DUNCAN, F. FITZMAURICE, A. GORDON, M. HENNESSY, J. HINCH, C. HICKEY, P. HJORTH, T. KYRKE-SMITH, D. LEAHY, W. LEE, E. LYNCH, O. MERCIER, S. MIKLAVCIC, S. RUSSELL, L. SCHWARTZ, B.F. SHOZI, P. SWIERCZYNSKI, C. TIMONEY, J. TOMCZYK, AND E. WARNEFORD, *Brewing of filter coffee*, Technical Report from MACSI's 2012 Problem-Solving Workshop with Industry, Limerick, Ireland, 2012.
- [3] E. BUSH, J. NIPKOW, B. JOSEPHY, S. HEUTLING, AND R. GRIESSHAMMER, *Strategies to enhance energy efficiency of coffee machines*, in EEDAL Conference, Vol. 75, Berlin, 2009.
- [4] R. J. CLARKE, *Extraction*, in Coffee, R. J. Clarke and R. Macrae, eds., Springer, The Netherlands, 1987, pp. 109–145.
- [5] A. FASANO, *Filtration problems in various industrial processes*, in Filtration in Porous Media and Industrial Application, A. Fasano, ed., Lecture Notes in Math. 1734, Springer, Berlin, Heidelberg, 2000, pp. 79–126.
- [6] A. FASANO AND A. FARINA, *Modelling complex flows in porous media by means of upscaling procedures*, Rend. Istit. Mat. Univ. Trieste, 42 (2010), pp. 65–102.

- [7] A. FASANO AND F. TALAMUCCI, *A comprehensive mathematical model for a multispecies flow through ground coffee*, SIAM J. Math. Anal., 31 (1999), pp. 251–273, <https://doi.org/10.1137/S0036141098336698>.
- [8] A. FASANO, F. TALAMUCCI, AND M. PETRACCO, *The espresso coffee problem*, in Complex Flows in Industrial Processes, A. Fasano, ed., Modeling and Simulation in Science, Engineering and Technology, Birkhäuser Boston, Boston, 2000, pp. 241–280.
- [9] C. GIANINO, *Experimental analysis of the Italian coffee pot “Moka”*, Amer. J. Phys., 75 (2007), pp. 43–47.
- [10] R. G. HOLDICH, *Fundamentals of Particle Technology*, Midland Information Technology and Publishing, Leistershire, UK, 2002.
- [11] A. ILLY AND R. VIANI, *Espresso Coffee: The Science of Quality*, Elsevier Academic, New York, 2005.
- [12] D. JAGANYI AND S. P. MADLALA, *Kinetics of coffee infusion: A comparative study on the extraction kinetics of mineral ions and caffeine from several types of medium roasted coffees*, J. Sci. Food Agric., 80 (2000), pp. 85–90.
- [13] M.-L. MATEUS, C. LINDINGER, J.-C. GUMY, AND R. LIARDON, *Release kinetics of volatile organic compounds from roasted and ground coffee: Online measurements by ptr-ms and mathematical modeling*, J. Agric. Food Chem., 55 (2007), pp. 10117–10128.
- [14] K. M. MORONEY, W. T. LEE, S. B. G. O’BRIEN, F. SUIJVER, AND J. MARRA, *Modelling of coffee extraction during brewing using multiscale methods: An experimentally validated model*, Chem. Engrg. Sci., 137 (2015), pp. 216–234.
- [15] K. M. MORONEY, W. T. LEE, S. B. G. O’BRIEN, F. SUIJVER, AND J. MARRA, *Coffee extraction kinetics in a well mixed system*, J. Math. Industry, 7 (2016), pp. 1–19.
- [16] L. NAVARINI, E. NOBILE, F. PINTO, A. SCHERI, AND F. SUGGI-LIVERANI, *Experimental investigation of steam pressure coffee extraction in a stove-top coffee maker*, Appl. Thermal Engrg., 29 (2009), pp. 998–1004.
- [17] M. PETRACCO, *Technology IV: Beverage Preparation: Brewing Trends for the New Millennium*, Blackwell Science Ltd., Oxford, UK, 2008, pp. 140–164.
- [18] G. PICTET, *Home and catering brewing of coffee*, in Coffee, R. J. Clarke and R. Macrae, eds., Springer, The Netherlands, 1987, pp. 221–256.
- [19] S. RAO, *Everything But Espresso: Professional Coffee Brewing Techniques*, S. Rao, available from <http://www.scottrao.com>, 2010.
- [20] S. SCHENKER, S. HANDSCHIN, B. FREY, R. PERREN, AND F. ESCHER, *Pore structure of coffee beans affected by roasting conditions*, J. Food Sci., 65 (2000), pp. 452–457.
- [21] M. SIVETZ AND H. E. FOOTE, *Coffee processing technology*, in Coffee Processing Technology, Vol. 2, Avi, Westport, CT, 1963.
- [22] J. A. M. SPANINKS, *Design Procedures for Solid-Liquid Extractors and the Effect of Hydrodynamic Instabilities on Extractor Performance*, Ph.D. thesis, Agricultural University of Wageningen, Wageningen, The Netherlands, 1979.
- [23] M. VAN DYKE, *Perturbation Methods in Fluid Mechanics*, Parabolic Press, Stanford, CA, 1975.
- [24] A. VOILLEY AND D. SIMATOS, *Modeling the solubilization process during coffee brewing*, J. Food Process Engrg., 3 (1979), pp. 185–198.